International Journal of Robotics and Automation (IJRA)
Vol. 6, No. 4, December 2017, pp. 286~302
ISSN: 2089-4856, DOI: 10.11591/ijra.v6i4.pp286-302

On the Design of a 4 Degrees-of-freedom Pick and Place Cable Suspended Parallel Manipulator

F. J. Castillo-Garcia[1], P. Rea[2], A. Gonzalez-Rodriguez[3], E. Ottaviano[4]
[1,3]School of Industrial Engineering, University of Castilla-La Mancha, Ciudad Real, Spain, Spanyol
[2,4]DICeM, University of Cassino and Southern Lazio, Italy

Article Info

Article history:

Received Aug 9, 2017
Revised Oct 20, 2017
Accepted Nov 4, 2017

Keyword:

Cable robot
Dynamic control
Kinematic
PD controller
Pick and place

ABSTRACT

This paper proposes the design and control strategy for a four degrees-of-freedom spatial cable-suspended parallel robot for pick and place operations. Pick and place is a repetitive task requiring payload changes for the movement to pick-up the object, and the movement to the final pose to release the manipulated object. In this paper, a new robust control strategy has been proposed, together with proper trajectories for the required operation. The control strategy consists on the system decoupling and linearization by means of a feedforward term and a cascade PD controller. The main advantage of the proposed solution is that its design can be scalable in size spanning from centimeters to meters with a relatively good positioning accuracy. Finally, simulations are reported to show the overall performances of the proposed configuration for pick and place operations with a medium size manipulator.

Corresponding Author:

F. J. Castillo-Garcia,
School of Industrial Engineering,
University of Castilla-La Mancha Real Fabrica de Armas,
Av. Carlos III, 13071 +34 902 204 100, Spanyol.
E-mail:fernando.castillo@uclm.es

1. INTRODUCTION

During the last two decades, the number of Pick and Place manipulators applications has significantly increased owing to the growing level of automation in all industrial areas. Pick and place can be considered the most common operation performed by a manipulator or an automatic system and it is defined as a repetitive task of pick up objects and place them somewhere else. Robots have been widely used for these operations, but the most implemented solution is the use of special manipulators speci cally designed for these operations. The Delta robot is often used to handle small products to larger items. The pioneer prototype was invented by Reymond Clavel in 1988 [1]. It consists of three symmetric kinematic chains of RRPaR, RUU or R (SS) 2 type, being R: revolute, U: universal, S: spherical, Pa: parallelogram joints. The robot architecture was designed to restrain completely the orientation of the mobile platform, which remains with three purely translational degrees of freedom. The Delta robot was designed for rapid movements, based on it several works have been subsequently presented [2-5]. A comprehensive overview can be found in [6].

In the last decades Cable-Driven Parallel Robots (CDPRs) have been developed and used as e - cient alternatives for some applications to the classical parallel robots [7]. CDPRs are a class of parallel manipulators [8] in which rigid links are replaced by cables, and the end-e ector is commanded by means of m cables with n actuators. Some advantages of this kind of manipulators are that they can be lighter, faster, safer, and more economical than traditional parallel ones (see e.g. [9-11]).

The number of applications of these robots has notoriously increased during the last years. Starting from the NIST RoboCrane system [12], originally designed for large-scale handling, cable-driven robots were designed to be used in a broad range of areas as: automation in construction [13-15], wind tunnels [16],

rehabilitation and motion aiding systems [17-19], scaffold systems for aircraft maintenance [20]. CDPRs are classified as fully constrained if, once the actuators are locked, the mobile platform pose is completely determined. They are underconstrained if the platform is movable when the cable lengths are assigned. In a cable-suspended robot (CSPR), all cables lie above the moving platform and the end-e ector, payload or tool, can be positioned (e.g. [21, 22]) and/or oriented (e.g. [23]) into its workspace being suspended, indeed they can be considered as crane-type manipulators [24, 25]. Orientation capabilities of CDPRs can be also improved by coupling it with a parallel spherical wrist actuated by cable-driven omni-wheels, as described in [26].

CSPRs have great potentialities for many applications, in fact, if all the fixed attachment points are located above the workspace, then cables do not clutter the part of the robot workspace located below the platform. This occurrence drastically reduces the possible interference among cables, end-e ector, and environment, but the positioning capability is strictly related to the gravity and then to the solution of the static problem. Moreover, external disturbances on the end-e ector determine complex dynamics involving cable vibrations.

Main problem of CSPR is related to the nature of the robot, the suspended end-e ector is prone to vibrations and sensitive to external disturbances. These factors, together with complex Kinetostatics and Dynamics, my greatly limit their usability.

Works on statics and dynamics of cable-suspended robots are reported in [27, 28]. Vibration occurrences was studied in fully-constrained manipulators by considering cables as linear or nonlinear springs such as in [29, 30] or CSPRs [31].

Pick and place operation is quite common industrial repetitive task involving a motion towards an object, picking and moving to another place to release it. Therefore, the robotic arm will move with a variable mass (with and without an object) during the operation involving important dynamic e ects. These issues are much more relevant when CSPRs are involved.

This paper details issues of a 4DOF spatial cable-suspended robot to be used for pick and place operations. Since this task requires that the robot payload changes, a robust control must be developed in order to provide a high performance trajectory tracking.

This paper is organized as follows: Section 2 details the cable-suspended Kinematics and Dynamics for the proposed spatial CSPR. Section 3 introduces the trajectories implemented for pick and place operations. Section 4 reports the proposed control scheme. Section 5 presents simulation results, and finally, Section 6 summarizes the main conclusions.

2. MODELING

2.1 8-4 Cable Suspended Robot Description

As it was shown in the design solution proposed in [21], and successfully applied in [17], if the end-effector is suspended by means of pairs of parallel cables, the orientation of the end-e ector remains unchanged. In this paper, a Cable Suspended Parallel Robot, hereafter CSPR, is considered having 8 cables arranged in parallel by pairs, each pair having the same length and being commanded by 4 motors, one for each pair of cables [32]. In particular, each pair of cables, together with the frame and the end-effector, constitutes a parallelogram, as it is shown in the scheme of Figure 1.

According to 1a W is the width of the frame (along X axis), L its length (along Y axis) and H is the height (along Z axis), the same holds for the end-effector, being w, l and h, wide, length and height, respectively. T_{iu} and T_{il} are the tensions of the upper and lower cables of the *i*-th pair, respectively. The colored regions show each parallelogram constituted by two fixed points placed at the frame and two points placed at the end-effector, as it is shown in Figure 1. The architecture based on the geometry of parallelograms restrains the orientation of the end-effector, leaving only one rotation about Z-axis. Therefore, end-effector pose is given by $Q = [x, y, z, \delta]^T$, being the orientation angle with respect to Z axis. Therefore, this CSPR configuration has 4 actuators to provide 4 DOFs. It is worth noting that this holds if $\frac{w}{l} \neq \frac{W}{L}$, otherwise rotation about *Z* axis is also not allowed, as it is reported in [21].

The frame and the end-effector are therefore connected by means of 4 pairs of cables going from fixed points at the frame, $Q_i^f = [x_i^f, y_i^f, z_i^f]^T$, to each respective end-effector anchor points, $Q_i^e = [x_i^e, y_i^e, z_i^e]^T$, as shown Figure 1 being Q_{fi} fixed points, while Q_{ei} depend by the end-effector pose, *Q*. Table 1 summarizes x_i^f, y_i^f and z_i^f coordinates of all frame node connections.

Finally, the direction of the *i*-th cable can be represented by means of angles θ_i, with regards to Y-axis, and ϕ_i, with respect to Z-axis as shown in Figure 1b. The active angle of the set gearbox-motor *i* is given by α_i as shown in Figure 1c, according to the design proposed in [32]

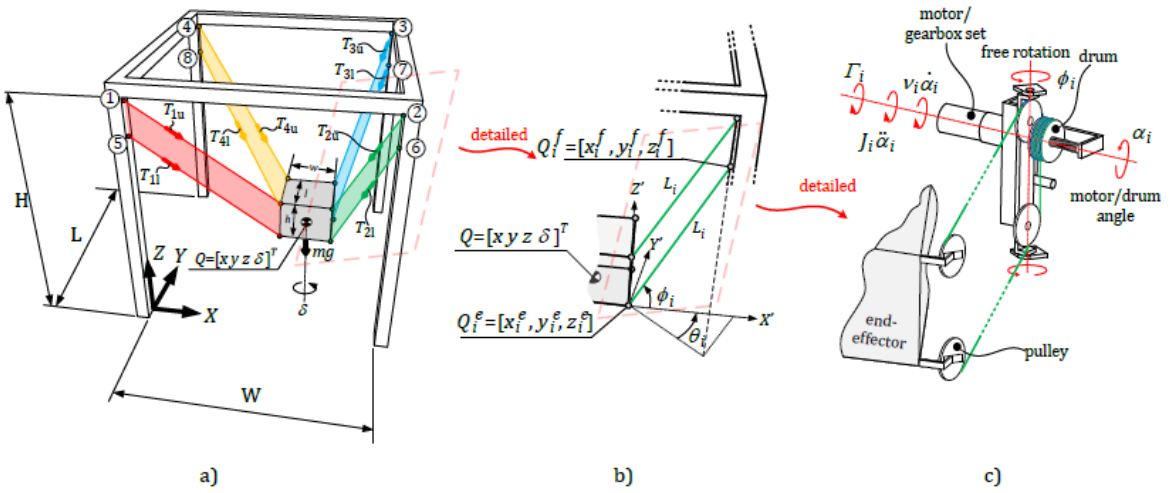

Figure 1. Scheme of the 8-4CSR design

Table 1. 8-4 CSR Design x_i^f, y_i^f, z_i^f, dx_i, dy_i and dz_i Values

i	*1*	*2*	*3*	*4*	*5*	*6*	*7*	*8*
x_i^f	*0*	*W*	*W*	*0*	*0*	*W*	*W*	*0*
y_i^f	*0*	*0*	*L*	*L*	*0*	*0*	*L*	*L*
z_i^f	*H*	*H*	*H*	*H*	*H-h*	*H-h*	*H-h*	*H-h*
dx_i	*w/2*	*w/2*	*-w/2*	*-w/2*	*w/2*	*w/2*	*-w/2*	*-w/2*
dy_i	*-l/2*	*l/2*	*l/2*	*-l/2*	*-l/2*	*l/2*	*l/2*	*-l/2*
dz_i	*h/2*	*h/2*	*h/2*	*h/2*	*-h/2*	*-h/2*	*-h/2*	*-h/2*

2.2 Inverse Kinematics

The Forward and Inverse Kinematics problem for CSPR are not trivial ones, as it is shown in [[24]]. The Forward Kinematics, Λ^F, relates the active joint angles, $\alpha = [\alpha_1, \alpha_2, \alpha_3, \alpha_4]^T$, to the end-effector Cartesian pose, $Q = [x, y, z, \delta]^T$, i.e., $Q=\Lambda^F(\alpha)$. The inverse kinematics, Λ^I, is the inverse transformation $\alpha = \Lambda^I(Q)$.

For a given end-effector pose, Q, Q_i^e points can be determined by (1)

$$\mathbf{Q}_i^e = \mathbf{Q} + \begin{bmatrix} \cos(\delta) & -\sin(\delta) & 0 \\ \sin(\delta) & \cos(\delta) & 0 \\ 0 & 0 & 1 \end{bmatrix} \begin{bmatrix} dx_i \\ dy_i \\ dz_i \end{bmatrix} \tag{1}$$

where dx_i, dy_i and dz_i are fixed values of the proposed robot configuration and are summarized in Table 1. Once that Qei is obtained, angles i and i can be expressed as (2)

$$\begin{aligned} \theta_i &= \tan^{-1}\left(\frac{y_i^f - y_i^e}{x_i^f - x_i^e}\right) \\ \phi_i &= \tan^{-1}\left(\frac{z_i^f - z_i^e}{\sqrt{(x_i^f - x_i^e)^2 + (y_i^f - y_i^e)^2}}\right) \end{aligned} \tag{2}$$

It is worth noting that the Jacobian matrix is usually expressed as function of cables angles, θ_i and ϕ_i. On the other hand, considering sets gearbox/motor angles at home position $\alpha_i = 0$, when the end-effector is placed at the fixed frame centroid and $\delta_0 = 0$ orientation, $Q_0 = [x_0, y_0, z_0, \delta_0]^T = [W/2, L/2, H/2, 0]^T$, the initial length of all cables, L^0, can be obtained as (3)

$$\begin{aligned} L^0 &= L_{iu}^0 = L_{il}^0 = \\ &= \tfrac{1}{2}\sqrt{(W-w)^2 + (L-l)^2 + (H-h)^2} \end{aligned} \tag{3}$$

Denoting $L_i = L_{iu} = L_{id}$ and given an end-effector pose, Q, cables length yield as (4)

$$L_i = \sqrt{\left(x_i^f - x_i^e\right)^2 + \left(y_i^f - y_i^e\right)^2 + \left(z_i^f - z_i^e\right)^2} \tag{4}$$

At this kinematic configuration, positive angles changes on the the set motor/gearbox/drum α_i, cause positive changes in the cables length, $\Delta L_{iu} = \Delta L_{il}$ and the cable length variations can be therefore expressed as $\Delta L_{iu} = \Delta L_{il} = \alpha_i r$, where r is the last pulley/drum radius. In this way, actuator sets angles can be obtained as (5)

$$\boldsymbol{\alpha} = \frac{1}{r}\mathbf{\Delta L} \tag{5}$$

where $\mathbf{\Delta L} = [\Delta L_1, \Delta L_2, \Delta L_3, \Delta L_4]^T = \left[L_1 - L^0,\ L_2 - L^0, L_3 - L^0\ L_4 - L^0\right]^T$. Combining (3), (4) and (5), the Inverse Kinematics, $\mathbf{\Lambda}^{\mathrm{I}}$ can be expressed as (6)

$$\alpha_i = \frac{\sqrt{\left(x_i^f - x_i^e\right)^2 + \left(y_i^f - y_i^e\right)^2 + \left(z_i^f - z_i^e\right)^2} - L^0}{r} \tag{6}$$

for i = 1, 2, 3, 4.

The control strategy for end-effector trajectory tracking, proposed in Section 3, requires the use of the inverse kinematics, $\mathbf{\Lambda}^{\mathrm{I}}$, but does not the use of the forward one $\mathbf{\Lambda}^{F}$.

2.3 End-effector dynamic model

The static equilibrium of the end-effector can be expressed as (7)

$$\mathbf{M}\ddot{\mathbf{Q}} = \mathbf{F} \tag{7}$$

Where (8)

$$\mathbf{M} = \begin{bmatrix} m & 0 & 0 & 0 \\ 0 & m & 0 & 0 \\ 0 & 0 & m & 0 \\ 0 & 0 & 0 & I_z \end{bmatrix} \tag{8}$$

Being m the end-effector mass, I_z the moment of inertia with respect to Z axis and $\mathrm{F} = [\mathrm{F}_x, \mathrm{F}_y, \mathrm{F}_z, \Gamma_z]^{\mathrm{T}}$ is the cartesian forces and torque array applied on the end-effector by the actions of the cables tension and the gravity, i.e (9)

$$\mathbf{F} = \mathbf{J_s}\mathbf{T} + \begin{bmatrix} 0 \\ 0 \\ -mg \\ 0 \end{bmatrix} \tag{9}$$

In (9), T is the cable tension array $\mathrm{T} = [T_1, T_2, T_3, T_4]^{\mathrm{T}}$ being $T_i = T_{iu} + T_{id}$ for i = 1, 2, 3, 4, and $\mathbf{J}_{\mathrm{s}}$ is the static Jacobian which yields as (10)

$$\mathbf{J}_s = \begin{bmatrix} J_{11} & J_{12} & J_{13} & J_{14} \\ J_{21} & J_{22} & J_{23} & J_{24} \\ J_{31} & J_{32} & J_{33} & J_{34} \\ J_{41} & J_{42} & J_{43} & J_{44} \end{bmatrix} \tag{10}$$

Being (11)

$$\begin{aligned} J_{1i} &= \cos(\phi_i)\cos(\theta_i) \\ J_{2i} &= \cos(\phi_i)\sin(\theta_i) \\ J_{3i} &= \sin(\phi_i) \\ J_{4i} &= d\left(\cos\left(\theta_{i0} + \delta\right)\cos\left(\phi_i\right)\sin\left(\theta_i\right)\right. \\ &\quad \left. - \sin\left(\theta_{i0} + \delta\right)\cos\left(\phi_i\right)\cos\left(\theta_i\right)\right) \end{aligned} \tag{11}$$

where $\theta_{i0} = \tan^{-1}\left(\frac{dy_i}{dx_i}\right)$ and $d = \frac{\sqrt{w^2+l^2+h^2}}{2}$.

2.4 Motor Dynamics Model

According to the scheme in Figure 1c the dynamics of the sets motor/gearbox/drum can be described by (12)

$$\mathbf{J}\ddot{\boldsymbol{\alpha}} + \boldsymbol{\nu}\dot{\boldsymbol{\alpha}} = \boldsymbol{\tau} - r\mathbf{T} \tag{12}$$

where **J** is the rotational inertia matrix (13)

$$\mathbf{J} = \begin{bmatrix} J_1 & 0 & 0 & 0 \\ 0 & J_2 & 0 & 0 \\ 0 & 0 & J_3 & 0 \\ 0 & 0 & 0 & J_4 \end{bmatrix} \tag{13}$$

v is the viscous friction coefficients matrix (14)

$$\boldsymbol{\nu} = \begin{bmatrix} \nu_1 & 0 & 0 & 0 \\ 0 & \nu_2 & 0 & 0 \\ 0 & 0 & \nu_3 & 0 \\ 0 & 0 & 0 & \nu_4 \end{bmatrix} \tag{14}$$

r the drum/pulleys radius and $\boldsymbol{\tau} = [\tau_1, \tau_2, \tau_3, \tau_4]^T$ is the motors torque array (input signal).

2.5 System dynamics

Rearranging (12), cables tensions can be expressed as (15)

$$\mathbf{T} = \frac{1}{r}\left(\boldsymbol{\tau} - \mathbf{J}\ddot{\boldsymbol{\alpha}} - \boldsymbol{\nu}\dot{\boldsymbol{\alpha}}\right) \tag{15}$$

that can be substituted in (9) and introduced in (7) yielding (16)

$$\mathbf{M}\ddot{\mathbf{Q}} = \mathbf{J_s}\frac{\mathbf{1}}{\mathbf{r}}\left(\boldsymbol{\tau} - \mathbf{J}\ddot{\boldsymbol{\alpha}} - \boldsymbol{\nu}\dot{\boldsymbol{\alpha}}\right) + \begin{bmatrix} 0 \\ 0 \\ -mg \\ 0 \end{bmatrix} \tag{16}$$

System dynamics behavior described by (16) that can be expressed in Cratesian coordinates, Q, as (17)

$$\mathbf{M}\ddot{\mathbf{Q}} = \mathbf{J_s}\frac{\mathbf{1}}{\mathbf{r}}\left(\boldsymbol{\tau} - \mathbf{J}\ddot{\boldsymbol{\Lambda}}^{\mathbf{I}}(\mathbf{Q}) - \boldsymbol{\nu}\dot{\boldsymbol{\Lambda}}^{\mathbf{I}}(\mathbf{Q})\right) + \begin{bmatrix} 0 \\ 0 \\ -mg \\ 0 \end{bmatrix} \tag{17}$$

or in joint coordinates, α, as (18)

$$\mathbf{M}\ddot{\boldsymbol{\Lambda}}^{\mathbf{F}}(\boldsymbol{\alpha}) = \mathbf{J_s}\frac{\mathbf{1}}{\mathbf{r}}\left(\boldsymbol{\tau} - \mathbf{J}\ddot{\boldsymbol{\alpha}} - \boldsymbol{\nu}\dot{\boldsymbol{\alpha}}\right) + \begin{bmatrix} 0 \\ 0 \\ -mg \\ 0 \end{bmatrix} \tag{18}$$

Note that (15) is only valid if all cables tensions remain positive and therefore, the validity of models (16), (17) or (18), depends on this assumption.

3. CONTROL STRATEGY

3.1 Control objectives

The control objectives for the proposed 8-4CSR on pick and place operations are: End-effector accurate trajectory tracking, i.e. $|\mathbf{Q} - \mathbf{Q}^*| < \epsilon$. Robustness to payload changes owing to the needed operation with and without payload, i.e. $m_e \leq m \leq \overline{m}$., where m_e is the end-effector mass and $\overline{m}$ is the add of the end-effector mass and the one of the weighter object to be manipulated.

3.2 Control scheme

The most of the works which deals with the control of cable-driven robot problem use (17), or slight modifications, as a dynamic model of the manipulator, where $\boldsymbol{\tau}$ is the input torque array and **Q** the end-effector pose, i.e., the output of the model (see e.g. [33]).

On the other hand, sensors which provide a real time measurement of the end-effector pose, in order to feedback it in the control scheme, are expensive and therefore the most extended and used solution consists of measuring the motors angular configuration, $\boldsymbol{\alpha}$, and to estimate the end-effector pose, **Q**, by means of the forward kinematics transformation, $\mathbf{Q} = \Lambda^F(\boldsymbol{\alpha})$. In this way, input signal to the controller is the tracking error, **E = Q* - Q**, since its output is the motors input torques, $\boldsymbol{\tau}$.

It is usual to nd mechanical solutions which synthesis are designed to make the system quasilinear, i.e, linear relation between actuation and tip position [34]. This solution is not feasible in cable robots and, in order to obtain an accurate end-effector trajectory tracking, some authors linearize the dynamics equation (17) feedforwarding the nonlinear term **N(Q, Q)** [35] or assuming it negligible [33].

In this paper, we propose a cascade *P D* controller with a feedforward term. Attending to (16), a new input signal $\bar{\boldsymbol{\tau}}$ can be designed as (19)

$$\bar{\boldsymbol{\tau}} = \boldsymbol{\tau} - \boldsymbol{\Xi}(\ddot{\mathbf{Q}}) \tag{19}$$

being $\boldsymbol{\Xi}(\ddot{\mathbf{Q}}) = -r\mathbf{J}_s^{-1}(\ddot{\mathbf{Q}} + \mathbf{A}_G)$, where A_G = [0, 0, -g; 0]^T. In this way, dynamics equation (16) can betherefore rewritten as (20)

$$m\bar{\tau}_i(t) = J_i\ddot{\alpha}_i + \nu_i\dot{\alpha}_i \tag{20}$$

for *i* = 1, …, 4. Note that (20) is a decoupled model for each actuator set, in which input signal is $\bar{\tau}_i$ which commands the actuators angle α_i. Applying Laplace transform to (20), the transfer function which relates actuators angle, $\alpha_i(s) = \mathcal{L}\{\alpha_i(t)\}$, to the input torque to the motor, $\bar{\tau}_i(s) = \mathcal{L}\{\bar{\tau}_i(t)\}$ yields (21)

$$\mathbf{G}(s) = \begin{pmatrix} G_1(s) & 0 & 0 & 0 \\ 0 & G_2(s) & 0 & 0 \\ 0 & 0 & G_3(s) & 0 \\ 0 & 0 & 0 & G_4(s) \end{pmatrix} \tag{21}$$

Where (22)

$$G_i(s) = \frac{\alpha_i(s)}{\bar{\tau}_i(s)} = \frac{A_i}{s(s + B_i)} \tag{22}$$

where $A_i = \frac{m}{J_i}$ and $B_i = \frac{\nu_i}{J_i}$. Note that the new input signal $\bar{\boldsymbol{\tau}}$, used to decoupled the model, needs **Q** and, as it was previously mentioned, no sensor is available to obtain a direct measure of the end-effector pose. Then, we find two possibilities to compute $\bar{\boldsymbol{\tau}}$: a) estimate it by means of $\boldsymbol{\alpha}$, that is directly measured by means of the motors encoders, and the forward kinematics, $\Lambda^F(\boldsymbol{\alpha})$, or b) use directly **Q*** instead of **Q**. We have chosen option b) owing to the difficulty of a real time computing of the forward kinematics, $\Lambda^F(\boldsymbol{\alpha})$. Figure 2 represents the block diagram of the proposed control strategy for obtaining an equivalent linear-decoupled model.

Using the linear-decoupled model shown in Figure 2, a conventional controller can be designed using any linear control techniques. Note that transfer function (22) is of the form of a DC-motor one (see e.g. [36]) and any strategy for DC-motor position control can be therefore applied. Due to the required robustness of the control system when payload changes, in this work we propose a cascade PD controller to obtain the required robust behavior. This technique has been successfully applied previously (see [36]).

Figure 3 represents the cascade *PD* controller embedded in the linearizing/decoupling strategy and its equivalent linear decoupled diagram block. This equivalent scheme will be used to tune the cascade PD controller.

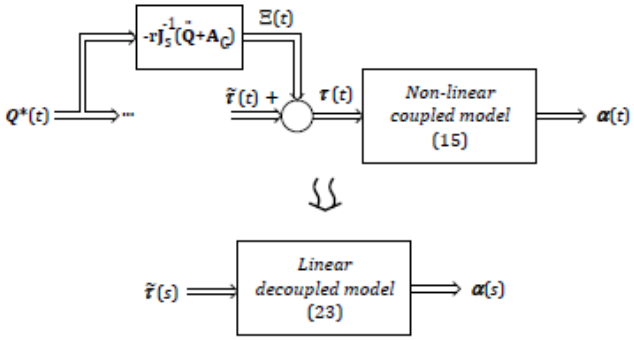

Figure 2. Proposed linearizing/decoupling strategy

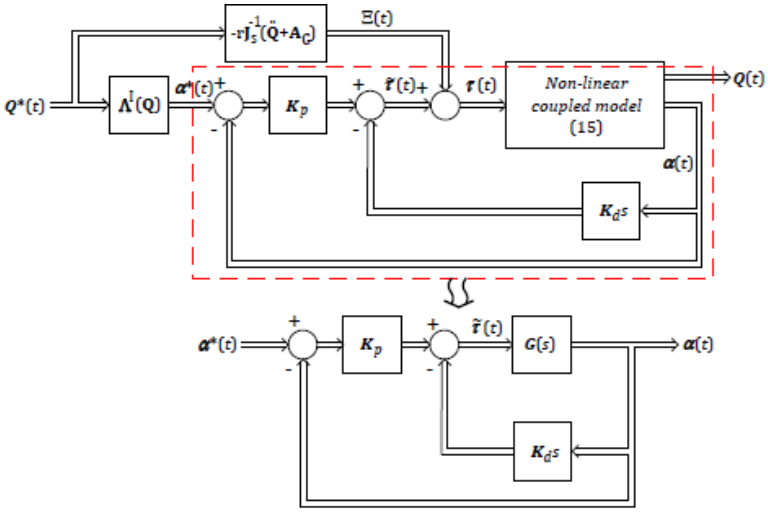

Figure 3. Cascade PD controller + linearizing/decoupling strategy

3.3 Controller tuning

In Figure 3 $\mathbf{K_p}$ and $\mathbf{K_d}$ are diagonal 4x4 matrixes which diagonal elements, $\mathbf{K_{pi}}$ and $\mathbf{K_{di}}$, are respectively designed for controlling $G_i(s)$. The closed loop transfer function of axis *i* can be written as (23)

$$M_i(s) = \frac{\alpha_i^*(s)}{\alpha_i(s)} = \frac{A_i K_{pi}}{s^2 + (B_i + A_i K_{pi})\, s + A_i K_{pi}} \tag{23}$$

and therefore, the equivalent open loop transfer function yields (24)

$$H_i(s) = \frac{A_i K_{pi}}{s\,(s + (B_i + A_i K_{di}))} \tag{24}$$

Note that applying the *Final Value Theorem* (see e.g. [37]), the steady state error of the closed loop transfer function is zero. In this way, the cascade PD controller can be tuned in order to control the time response velocity of the system and its overshoot. The conventional frequency requirements, gain crossover frequency, ω_c (related to the time response velocity) and phase margin, ϕ_m (related to the time response overshoot) are used to tune the proposed controller (see e.g. [37]). The complex tuning equation which fulfills the frequency requirements, ω_c and ϕ_m is

$$H_i(j\omega_c) = e^{-j(\pi - \phi_m)} \tag{25}$$

replacing (24) in (25), the controller tuning equations can be obtained and yield (26)

$$K_{pi} = \frac{\omega_c^2}{A_i \cos(\phi_m)}$$
$$K_{di} = \frac{\omega_c \tan(\phi_m) - B_i}{A_i} \quad (26)$$

The tuning procedure consists therefore on selecting proper values of the gain crossover frequency and phase margin and to use (26) to obtain the controllers parameters, K_{pi} and K_{di} for all motors (i = 1, 2, 3, 4). Some works have described the advantages of the use of the proposed cascade *PD* controller in comparison, for example, to the conventional *PID* controller. One of these advantages is its robustness behaviour when the payload changes, as it is required for our control scheme (see e.g. [36]).

4. TRAJECTORIES FOR PICK AND PLACE OPERATION

This Section describes the designed trajectories for pick and place operation with the proposed 8-4*CSR*. Denoting the reference trajectory as $\boldsymbol{Q}^*$, Figure 4 represents a scheme of a spatial trajectory for pick and place operation from $\mathbf{Q}^*_{\mathbf{a}} = [x^*_a, y^*_a, z^*_a, \delta^*_a]^T$ to $\mathbf{Q}^*_{\mathbf{b}} = [x^*_b, y^*_b, z^*_b, \delta^*_b]^T$. Figure 4 represents the proposed trajectory that is usually applied to pick and place operation (e.g. see [38]). This trajectory is characterized by providing a vertical orientation for both, picking and placing and it must be a C^2 continuously differentiable function.

In Figure 4, plane* is the one that contains points a and b and Z axis. Points 1 to 4 can be easily obtained by points a and b and h_i and b_i parameters. Let's define the path variable s along plane*. Regarding to this path variable, trajectory shown in Figure 4 can be expressed as (27)

$$\begin{cases} \tilde{x}^*(s) = \tilde{x}^*_a \\ \tilde{z}^*(s) = \tilde{z}^*_a + s \end{cases} \quad \text{if } 0 \le s < s_1$$
$$\begin{cases} \tilde{x}^*(s) = \sum_{i=0}^{5} \xi_i^{x2} s^i \\ \tilde{z}^*(s) = \sum_{i=0}^{5} \xi_i^{z2} s^i \end{cases} \quad \text{if } s_1 \le s < s_2$$
$$\begin{cases} \tilde{x}^*(s) = \tilde{x}^*_2 + (s - s_2) \\ \tilde{z}^*(s) = \tilde{z}^*_2 \end{cases} \quad \text{if } s_2 \le s < s_3$$
$$\begin{cases} \tilde{x}^*(s) = \sum_{i=0}^{5} \xi_i^{x4} s^i \\ \tilde{z}^*(s) = \sum_{i=0}^{5} \xi_i^{z4} s^i \end{cases} \quad \text{if } s_3 \le s < s_4$$
$$\begin{cases} \tilde{x}^*(s) = \tilde{x}^*_4 \\ \tilde{z}^*(s) = \tilde{z}^*_4 - (s - s_4) \end{cases} \quad \text{if } s_5 \le s < s_b \quad (27)$$

where $\xi_i^{x2}, \xi_i^{y2}, \xi_i^{x4}$ and ξ_i^{y4} coefficients can be attained giving the following constraints (28)

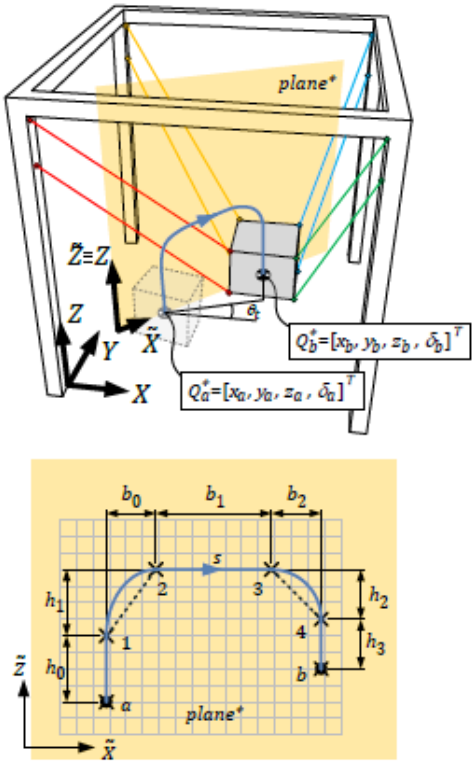

Figure 4. 8-4 CSR Trajectories description for pick and place operations

$$\begin{array}{lll}
\tilde{x}^*(s_1)=\tilde{x}_1^* & \tilde{x}^{*'}(s_1)=0 & \tilde{x}^{*''}(s_1)=0 \\
\tilde{z}^*(s_1)=\tilde{z}_1^* & \tilde{z}^{*'}(s_1)=1 & \tilde{z}^{*''}(s_1)=0 \\
\tilde{x}^*(s_2)=\tilde{x}_2^* & \tilde{x}^{*'}(s_2)=1 & \tilde{x}^{*''}(s_2)=0 \\
\tilde{z}^*(s_2)=\tilde{z}_2^* & \tilde{z}^{*'}(s_2)=0 & \tilde{z}^{*''}(s_2)=0 \\
\tilde{x}^*(s_3)=\tilde{x}_3^* & \tilde{x}^{*'}(s_3)=1 & \tilde{x}^{*''}(s_3)=0 \\
\tilde{z}^*(s_3)=\tilde{z}_3^* & \tilde{z}^{*'}(s_3)=0 & \tilde{z}^{*''}(s_3)=0 \\
\tilde{x}^*(s_4)=\tilde{x}_4^* & \tilde{x}^{*'}(s_4)=0 & \tilde{x}^{*''}(s_4)=0 \\
\tilde{z}^*(s_4)=\tilde{z}_4^* & \tilde{z}^{*'}(s_4)=-1 & \tilde{z}^{*''}(s_4)=0
\end{array} \tag{28}$$

Once that trajectory is defined in plane*, in XY Z it yields (29)

$$\begin{aligned}
x^*(s) &= \tilde{x}(s) \\
y^*(s) &= y_a^* + (\tilde{x}^*(s) - x_a^*)\tan(\theta_t) \\
z^*(s) &= \tilde{z}^*(s) \\
\delta^*(s) &= \delta_a^* + \tfrac{s-s_a}{s_b-s_a}(\delta_b^* - \delta_a^*)
\end{aligned} \tag{29}$$

where $\theta_t = \tan^{-1}\left(\frac{y_b^*-y_a^*}{x_b^*-x_a^*}\right)$. Note that a linear pro le has been added for expressing $\delta^*(s)$. In order to ensure that $x^*(t)$, $y^*(t)$, $z^*(t)$ and $\delta^*(t)$ are C^2 continuously differentiable functions, path variable s has been parameterized by a 3*th* order *Bezier* function. In order to avoid a possible loss of cables tension, the maximum Z axis deceleration has been limited to $\ddot{z} > -0.8g = -7.85\ \mathrm{m/s^2}$ by increasing the trajectory time. Figure 5 shows an the illustrative example of a trajectory from $\mathbf{Q_a}$ = [0.2m, 0.23m, 0.3m, -7°] to $\mathbf{Q_b}$ = [0.7m, 0.72m, 0.42m, 10°] with $h_0 = h_1 = b_0 = b_1 = b_2 = 0.1$m.

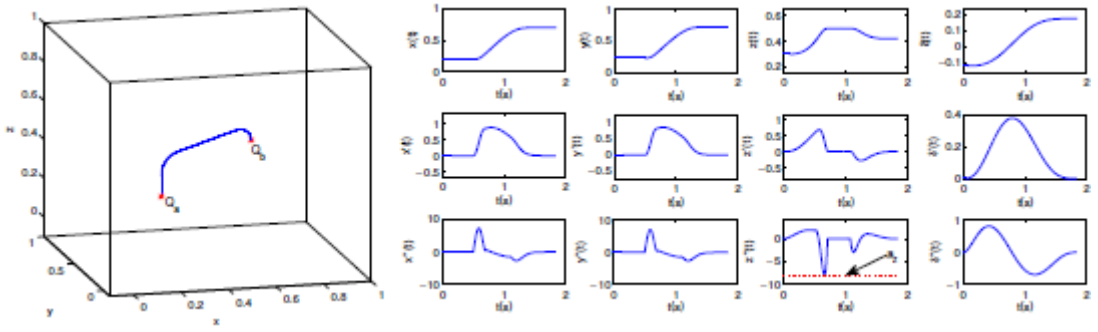

Figure 5. Example of pick and place trajectory: Spatial path, *x*(t), y*(t), z*(t)* and δ*(t)

5. SIMULATION RESULTS

5.1 Model parameters and dynamics validation

The 8-4*CSPR* model parameters used for simulations are summarized in Table 2.

Table 2. Parameters of the Proposed 8-4CSR Model Using in Simulations

Frame			
W (m)	*L (m)*	*H (m)*	
1.2	1.2	1.2	
End-effector			
w(m)	*l(m)*	*W (m)*	m_e*(Kg)*
0.1	0.2	0.2	1
Motor/gerabox/drum set			
J_i*(Kg/m^2)*	v_i*(Nms)*	*r(m)*	
2.6 10^{-4}	2.1 10^{-2}	0.075	

A dynamic model has been simulated using Matlab/Simulink. In order to validate it for the 8-4 CSPR an analogous model of the robot has been built using the multibody dynamics simulation software *MSC-ADAMs*.

Multiple scenarios have been simulated in order to check the validity of the *Matlab/Simulink* model. Figure 6 compares the results that Matlab/Simulink and *MSC-ADAMs* models provide for a initial pose of the end-effector, $\mathbf{Q_0}$ = [0.6m, 0.6m, 0.2m, 0^o], and the following step torques applied on each actuator, $\tau_1 = \tau^0$, $\tau_2 = \tau^0 + \Delta\tau$, $\tau_3 = \tau^0 + 2\Delta\tau$ and $\tau_4 = \tau^0 + 3\Delta\tau$, being $\tau^0 = 0.4956$ Nm and $\Delta\tau = 0.1$ Nm. Note that the error between *Matlab/Simulink* and *MSC-ADAMs* model for the simulation shown in Figure 6 is less than 2.10^{-4}. The sample time for the simulations has been set equal to T_s = 0.001 s.

5.2 Pick and place scenario

In order to check the proposed control strategy for our 8-4*CSPR*, a realistic scenario has been simulated. It consists on the robot initially placed on the centroid of the frame with zero orientation, $\mathbf{Q}_0 = [W/2, L/2, H/2, 0]^T$. It sequentially pick-up objects 1 to 5 from their initial poses, $\mathbf{Q}_{1a}$ ... $\mathbf{Q}_{5a}$, to their final ones, $\mathbf{Q}_{1b}$ ... $\mathbf{Q}_{5b}$ and come back to initial pose as it is indicated in Figure 7.

Table 3 summarizes the initial and final poses of the five objects and their mass. Note that during the robot manoeuvres the manipulator mass is the sum of end-effector mass, me, and each object mass, m_1, ..., m_5 during theirs respective trajectories.

5.3 Trajectories

Assuming that the initial and final poses of the end-effector are $\mathbf{Q_0}$ = [W/2, L/2, H/2, 0]^T, the described scenario demands 11 trajectories (first one: from 0 to 1a, second one: from 1a to 1b, third one: from 1b to 2a, ..., tenth one: from 5a to 5b, and the last one: from 5b to home). The trajectories detailed in Section 4 have been used to obtain the desired end-effector pose reference, $\mathbf{Q}$*(t). Figure 8 represents the Cartesian components of the required trajectory shown in Figure 7, and its Z axis acceleration. Note that its negative value has been limited to 80% of the gravity acceleration ($\underline{a}_Z$ > 0.8g), in order to ensure positive tension in all cables. This figure also shows the payload variation during the robot operation.

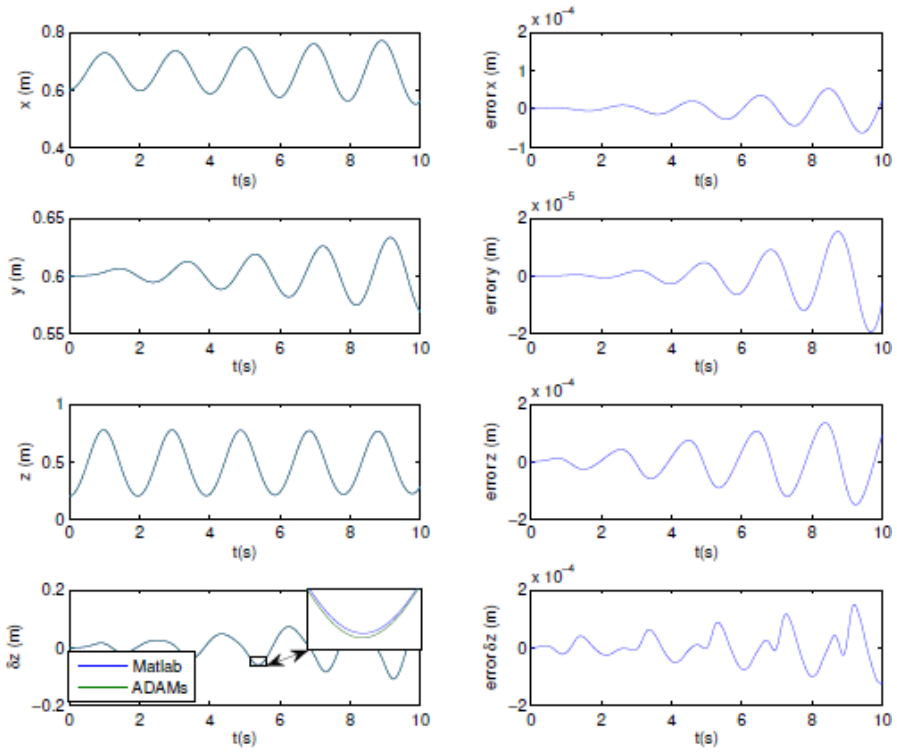

Figure 6. Matlab/Simulink vs. MSC-ADAMs: results

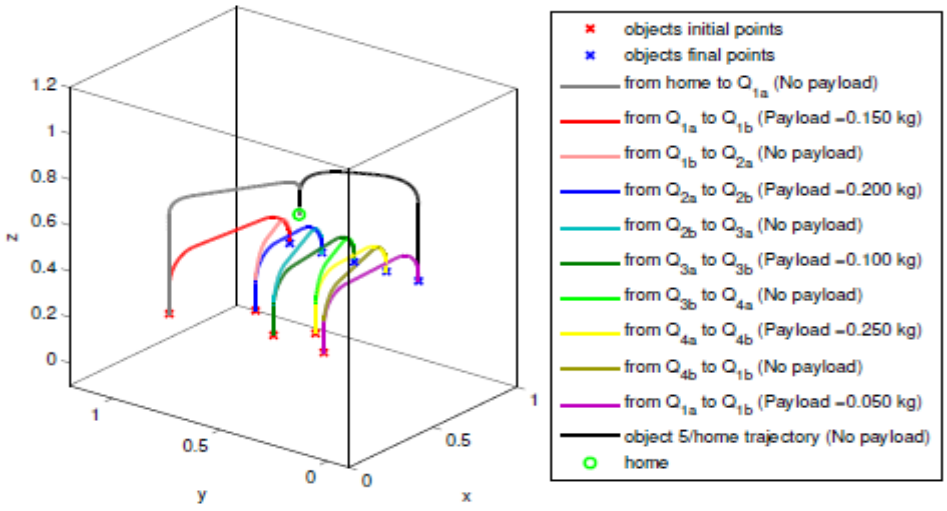

Figure 7. Spatial reference trajectory of the described scenario

Table 3. Simulation Scenario: Mass, Initial and Final Poses of the Objects.

	Initial pose, Q_a (m,°)				Final pose, Q_b (m,°)				mass
Object	x_a	y_a	z_a	δ_a	x_b	y_b	z_b	δ_b	(Kg)
1	0.16	0.86	0.25	-9	0.80	0.80	0.35	0	0.150
2	0.38	0.63	0.25	8	0.80	0.65	0.35	0	0.200
3	0.23	0.43	0.25	-4	0.80	0.50	0.35	0	0.100
4	0.34	0.32	0.25	6	0.80	0.35	0.35	0	0.250
5	0.21	0.18	0.25	-7	0.80	0.20	0.35	0	0.050

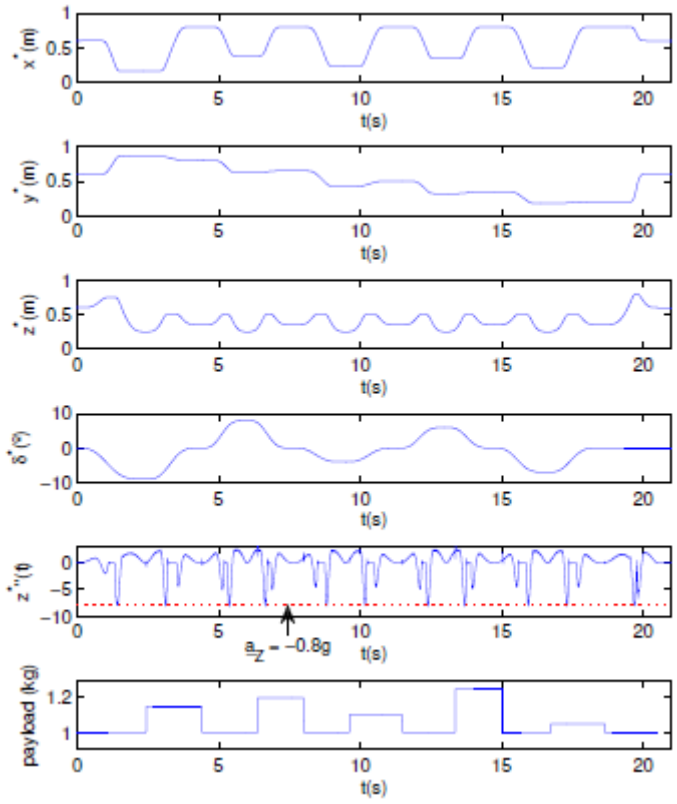

Figure 8. Reference trajectory, Z axis acceleration and payload variation of the described scenario

5.4 Controllers

Section 3 detailed the controller tuning procedure. After the feedforward term, $\Xi(\ddot{\mathbf{Q}}^*)$, the control strategy is based on tuning a cascade PD controller by means of the frequency domain speci cation gain crossover frequency, ω_c, and phase margin, m. A phase margin value, ϕ_m = 72° has been set in order to avoid overshoot in trajectory tracking (see e.g. [37]). On the other hand, a high value of the gain crossover frequency is required to diminish the delay between the reference trajectory and the end-effector pose. Based on simulations, an arbitrary value of ω_c = 260 rad/s has been set. Using the tuning equation (25), the four controllers (one per motor) are characterized by (30)

$$\begin{aligned} K_{pi} &= 40.46 \\ K_{di} &= 0.1537 \end{aligned} \tag{30}$$

5.5 Results

Figures 9 to 12 represent the simulation results of the described scenario. Figure 9 compares the reference trajectory, shown in Figure 8, and the end-effector pose.

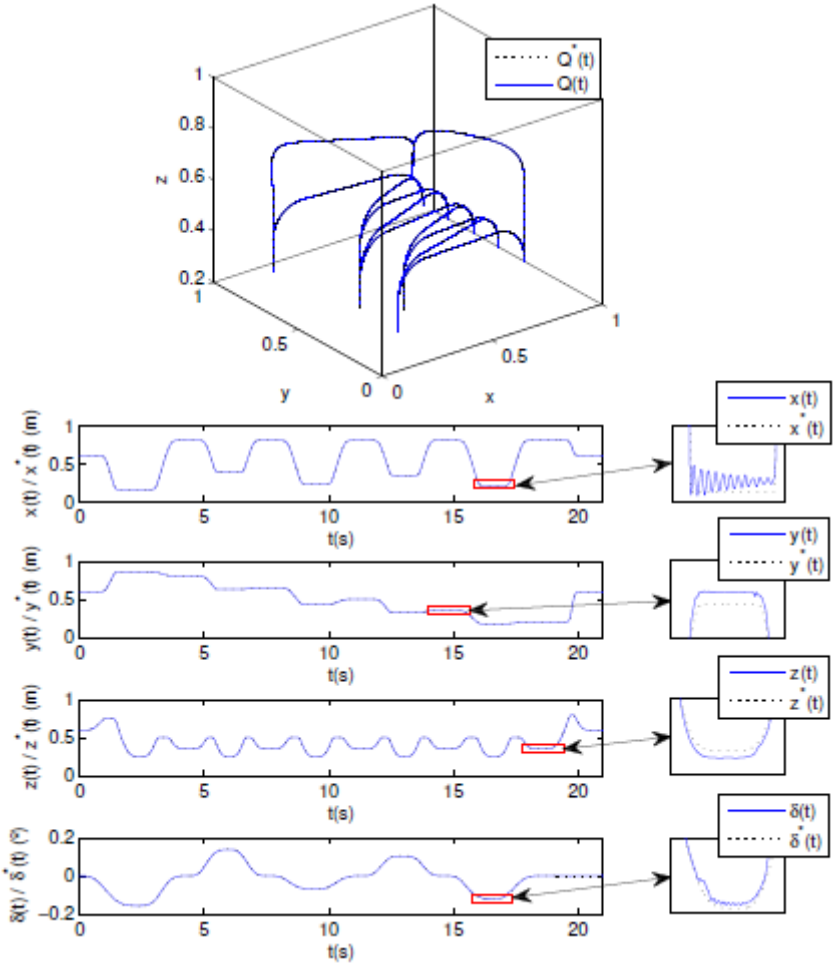

Figure 9. Reference trajectory and end-effector pose: trajectory tracking

Figure 10 represents the following tracking errors: $\epsilon_x = |x - x^*|$, $\epsilon_y = |y - y^*|$, $\epsilon_z = |z - z^*|$, $\epsilon_\delta = |\delta - \delta^*|$ and $\epsilon_Q = \sqrt{(x-x^*)^2 + (y-y^*)^2 + (z-z^*)^2}$. The results show that the tracking errors remains lower than 2.10^{-3}m in all cartesian components and lower than 0.5^o in orientation, independently of the payload. Figure 11 represents the control signal generated by controller (26) and the feedforward term, $\Xi(\ddot{\mathbf{Q}}^*)$. Finally, Figure 12 represents cables tension, T_1 to T_4. Note that all tension remains positive during the entire simulation, and therefore, dynamics model (16) can be considered valid.

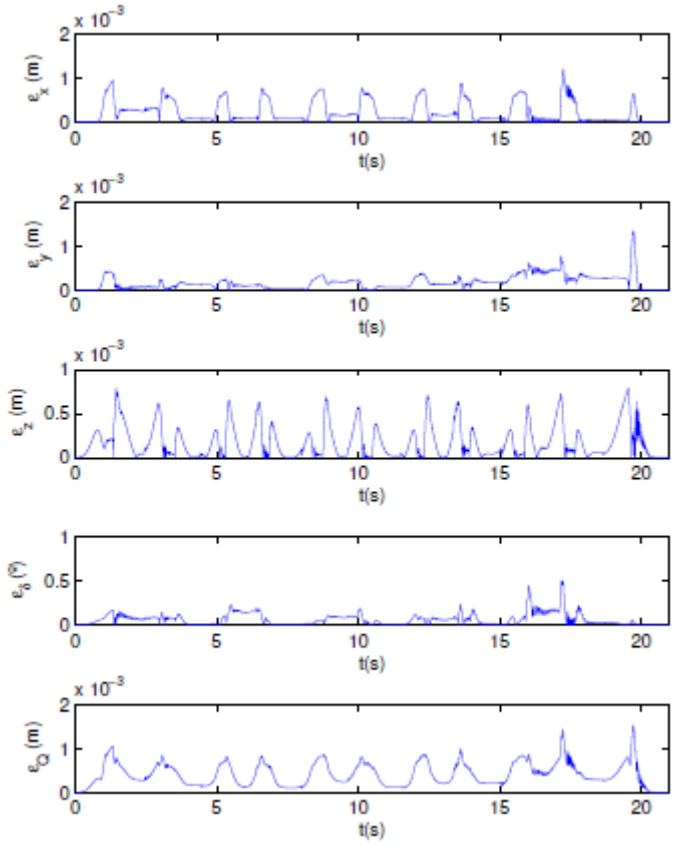

Figure 10. Tracking errors: ϵ_x, ϵ_y, ϵ_z, ϵ_δ ϵ_Q

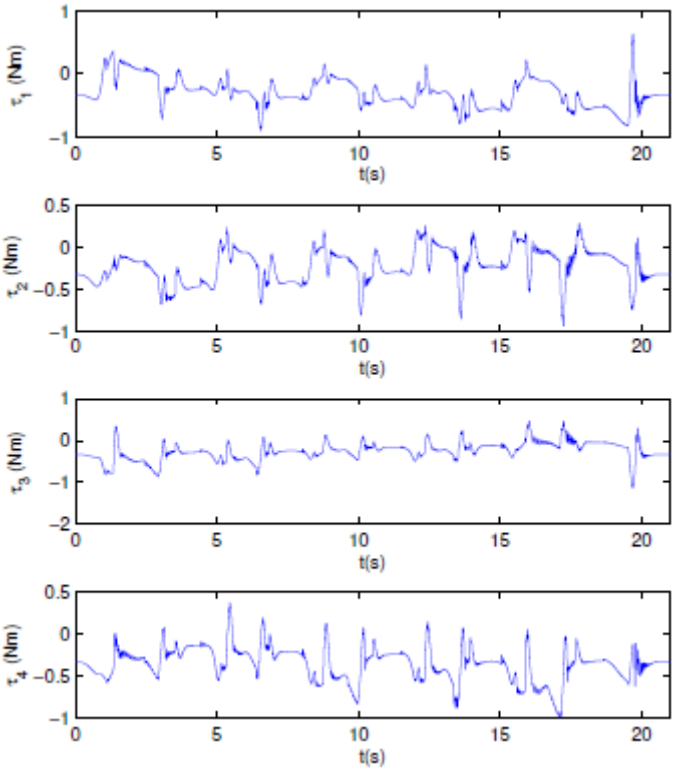

Figure 11. Control signal: motors' torque

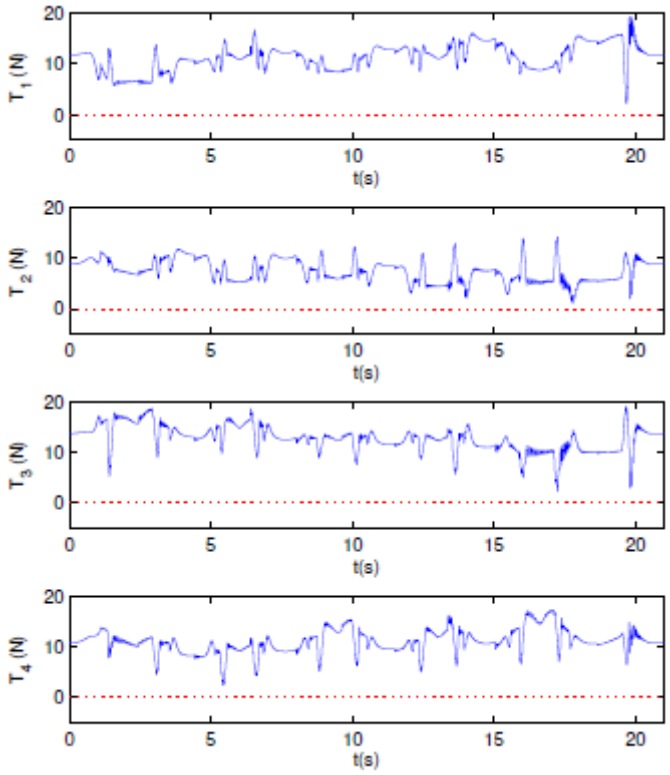

Figure 12. Reference trajectory, Z axis acceleration and payload variation of the described scenario

6. CONCLUSIONS

This paper proposes a novel control strategy for pick and place operation performed by cable suspended parallel manipulator. A 4 DOF spatial manipulator with 8 cables and 4 actuators has been considered. As the result, the main advantage of the proposed design and its control strategy is its high scalability and high payload capability. Proper trajectories have been designed taking into account the Z axis acceleration limit to ensure that all cables tension maintain positive values. The proposed novel control strategy consists on linearizing and decoupling the dynamics model by means of a simple feedforward term. Using the proposed technique the forward kinematics transform is no longer needed and any linear control strategy can be applied to design a proper controller.

Owing to the necessity of accurate trajectory tracking and robustness when payload changes, a cascade PD controller has been proposed tuned by a conventional frequency technique. Simulations results has been presented. Firstly, the Dynamics implemented on Maltab/Simulink has been compared to a pseudorealistic *MSC ADAMs* model. The results show a high level of equivalence between both models. Once that the developed model has been validated, a realistic scenario has been simulated. This scenario consists on picking and placing 5 objects, starting and ending at the initial pose.

These eleven trajectories were selected to span the robot workspace and have been satisfactory tracked with the proposed control strategy for large variation of the payloads. Results show a relatively good accuracy on the trajectory tracking (maximum error of about 1.5 10^{-3} m).Experimental validation of the proposed models has been also carried out. Figure 13 shows the built prototype.

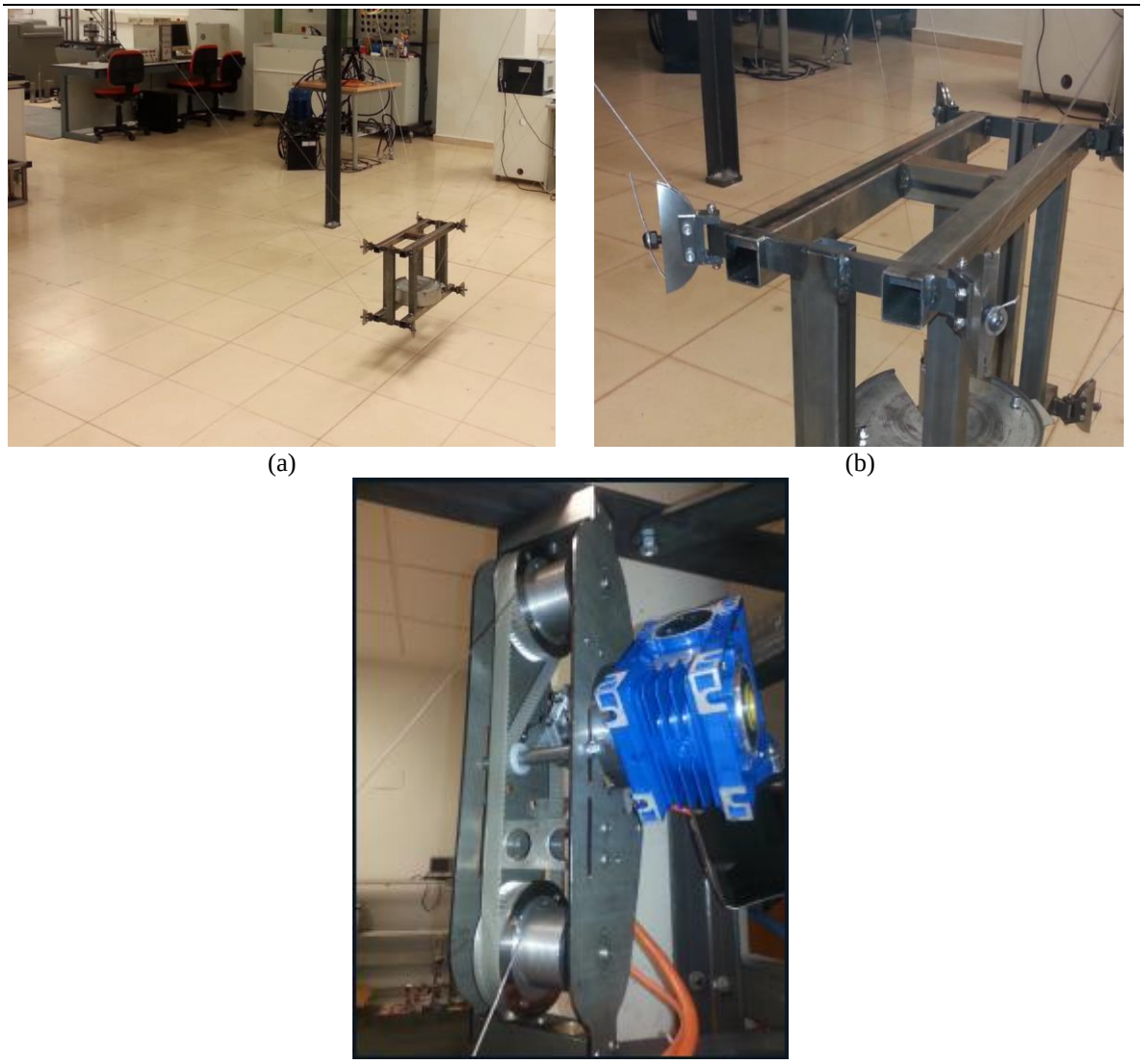

(a) (b)

(c)

Figure 13. a) Real prototype; b) End-effector pulleys; c) set motor/gearbox/drums

REFERENCES

[1] R. Clavel, “A fast robot with parallel geometry," in Proc. Int. Symposium on Industrial Robots, 1988, pp. 91{100.

[2] F. Pierrot, C. Reynaud, and A. Fournier, “Delta: a simple and e cient parallel robot," Robotica, vol. 8, no. 2, pp. 105{109, 1990.

[3] S. Briot, V. Arakelian, and V. Glazunov, “Design and analysis of the properties of the delta inverse robot," in Proceedings of the X International Conference on the Theory of Machines and Mechanisms, Liberec, Czech Republic, 2008.

[4] P. P. De Bie, “Load handling robot with three single degree of freedom actuators," Nov. 29 2016, uS Patent 9,505,139.

[5] B. Moharana, R. Gupta, and B. K. Kushwaha, “Optimization and design of a laser-cutting machine using delta robot," arXiv preprint arXiv:1404.6029, 2014.

[6] J. Brinker and B. Corves, “A survey on parallel robots with delta-like architecture," in Proceedings of the 14th IFToMM World Congress, 2015, pp. 407{414.

[7] A. Pott, H. Mutherich, W. Kraus, V. Schmidt, P. Miermeister, and A. Verl,”Ipanema: a family of cable-driven parallel robots for industrial applications," in Cable-Driven Parallel Robots. Springer, 2013, pp. 119{134.

[8] R. Verhoeven, “Analysis of the workspace of tendon-based stewart platforms," Ph.D. dissertation, Uni-versitat Duisburg-Essen, Fakultat fur Ingenieurwissenschaften Maschinenbau und Verfahrenstechnik, 2004.

[9] R. G. Roberts, T. Graham, and T. Lippitt, “On the inverse kinematics, statics, and fault tolerance of cable-suspended robots," Journal of Field Robotics, vol. 15, no. 10, pp. 581{597, 1998.

[10] I. Ebert-Upho and P. Voglewede, “On the connections between cable-driven parallel manipulators and grasping," in IEEE International Conference on Robotics and Automation, 2004, pp. 4521{4526

[11] S. Bouchard, C. Gosselin, and B. Moore, “On the ability of a cable-driven robot to generate a prescribed set of wrenches," Journal of Mechanisms and Robotics, vol. 2, no. 1, p. 011010, 2010.

[12] J. Albus, R. Bostelman, and N. Dagalakis, “The nist robocrane," Journal of Field Robotics, vol. 10, no. 5, pp. 709{724, 1993.
[13] A. Lytle, F. Proctor, and K. Saidi, “Control of cable robots for construction applications," in Parallel Manipulators, towards New Applications. InTech, 2008.
[14] P. Bosscher, R. L. Williams, L. S. Bryson, and D. Castro-Lacouture, \Cable-suspended robotic contour crafting system," Automation in Construction, vol. 17, no. 1, pp. 45{55, 2007.
[15] J.-B. Izard, M. Gouttefarde, C. Baradat, D. Culla, and D. Salle, \Integration of a parallel cable-driven robot on an existing building facade," in Cable-Driven Parallel Robots. Springer, 2013, pp. 149{164.
[16] C. Sturm, L. Wildan, and T. Bruckmann, “Wire robot suspension systems for wind tunnels," in Wind Tunnels and Experimental Fluid Dynamics Research. InTech, 2011.
[17] G. Castelli, E. Ottaviano, and P. Rea, “A cartesian cable-suspended robot for improving end-users' mobility in an urban environment," Robotics and Computer-Integrated Manufacturing, vol. 30, no. 3, pp. 335{343, 2014.
[18] M. J.-D. Otis, S. Perreault, T.-L. Nguyen-Dang, P. Lambert, M. Gouttefarde, D. Laurendeau, and C. Gosselin, “Determination and management of cable interferences between two 6-dof foot platforms in a cable-driven locomotion interface," IEEE Transactions on Systems, Man, and Cybernetics-Part A: Systems and Humans, vol. 39, no. 3, pp. 528{544, 2009.
[19] D. Surdilovic, J. Zhang, and R. Bernhardt, “String-man: Wire-robot technology for safe, exible and human-friendly gait rehabilitation," in Rehabilitation Robotics, 2007. ICORR 2007. IEEE 10th Inter-national Conference on. IEEE, 2007, pp. 446{453.
[20] D. Q. Nguyen and M. Gouttefarde, “Study of reconfigurable suspended cable-driven parallel robots for airplane maintenance," in Intelligent Robots and Systems (IROS 2014), 2014 IEEE/RSJ International Conference on. IEEE, 2014, pp. 1682{1689.
[21] G. Castelli, E. Ottaviano, and A. Gonzalez, “Analysis and simulation of a new cartesian cable-suspended robot," Proceedings of the Institution of Mechanical Engineers, Part C: Journal of Mechanical Engi-neering Science, vol. 224, no. 8, pp. 1717{1726, 2010.
[22] A. Trevisani, “Underconstrained planar cable-direct-driven robots: A trajectory planning method en-suring positive and bounded cable tensions," Mechatronics, vol. 20, no. 1, pp. 113{127, 2010.
[23] E. Ottaviano, “Analysis and design of a four-cable-driven parallel manipulator for planar and spatial tasks," Proceedings of the Institution of Mechanical Engineers, Part C: Journal of Mechanical Engi-neering Science, vol. 222, no. 8, pp. 1583{1592, 2008.
[24] M. Carricato and J.-P. Merlet, “Stability analysis of underconstrained cable-driven parallel robots," IEEE Transactions on Robotics, vol. 29, no. 1, pp. 288{296, 2013.
[25] M. Gouttefarde, J.-F. Collard, N. Riehl, and C. Baradat, “Geometry selection of a redundantly actuated cable-suspended parallel robot," IEEE Transactions on Robotics, vol. 31, no. 2, pp. 501{510, 2015.
[26] A. Platis, T. Rasheed, P. Cardou, and S. Caro, “Isotropic design of the spherical wrist of a cable-driven parallel robot," in Advances in Robot Kinematics 2016. Springer, 2018, pp. 321{330.
[27] K. Kozak, Q. Zhou, and J. Wang, “Static analysis of cable-driven manipulators with non-negligible cable mass," IEEE Transactions on Robotics, vol. 22, no. 3, pp. 425{433, 2006.
[28] J. Du and S. K. Agrawal, “Dynamic modeling of cable-driven parallel manipulators with distributed mass exible cables," Journal of Vibration and Acoustics, vol. 137, no. 2, p. 021020, 2015.
[29] S. Behzadipour and A. Khajepour, “Stiffness of cable-based parallel manipulators with application to stability analysis," Journal of mechanical design, vol. 128, no. 1, pp. 303{310, 2006.
[30] X. Diao and O. Ma, “Vibration analysis of cable-driven parallel manipulators," Multibody system dy-namics, vol. 21, no. 4, pp. 347{360, 2009.
[31] H. Yuan, E. Courteille, M. Gouttefarde, and P.-E. Herve, “Vibration analysis of cable-driven parallel robots based on the dynamic stiffness matrix method," Journal of Sound and Vibration, vol. 394, pp. 527{544, 2017.
[32] A. Gonzalez-Rodriguez, F. Castillo-Garcia, E. Ottaviano, P. Rea, and A. Gonzalez-Rodriguez, “On the e ects of the design of cable-driven robots on kinematics and dynamics models accuracy," Mechatronics, vol. 43, pp. 18{27, 2017.
[33] R. L. Williams II, “Cable-suspended haptic interface," International Journal of Virtual Reality, vol. 3, no. 3, pp. 13{21, 1998.
[34] A. Gonzalez Rodriguez, A. Gonzalez Rodriguez, and P. Rea, “A new articulated leg for mobile robots," Industrial Robot: An International Journal, vol. 38, no. 5, pp. 521{532, 2011.
[35] P. Gallina, A. Rossi, and R. L. Williams II, “Planar cable-direct-driven robots, part ii: Dynamics and control," in ASME. DECT2001 ASME Design Engineering Technical Conference. Pittsburgh: ASME Publisher, vol. 2, 2001, pp. 1241{1247.
[36] V. Feliu, F. J. Castillo, F. Ramos, and J. A. Somolinos, “Robust tip trajectory tracking of a very lightweight single-link exible arm in presence of large payload changes," Mechatronics, vol. 22, no. 5, pp. 594{613, 2012.
[37] K. Ogata, “Modern control engineering," Book Reviews, vol. 35, no. 1181, p. 1184, 1999.
[38] T. Huang, P. Wang, J. Mei, X. Zhao, and D. Chetwynd, “Time minimum trajectory planning of a 2-dof translational parallel robot for pick-and-place operations," CIRP Annals-Manufacturing Technology, vol. 56, no. 1, pp. 365{368, 2007.